J Mater Sci (2009) 44:3273–3284
DOI 10.1007/s10853-009-3443-6

TiB_2-reinforced composite coating by gas tungsten arc welding

S. O. Yilmaz · M. Ozenbas

Received: 28 September 2008 / Accepted: 27 March 2009 / Published online: 15 April 2009

Abstract In situ synthesized TiB_2-reinforced Fe-based coating was fabricated by gas tungsten arc welding (GTAW) on AISI-4340 steel substrate using cheaper Fe–Ti, Fe–Cr, Fe–W, Fe–B alloys and B_2O_3 powders. The effects of processing parameters on the coating were investigated experimentally. Primary dendrites of ferrite (α) phase and complex TiB_2, Fe_2B borides were detected at the coated surface. The experimental results show that either coated surface or interface microstructures were formed by the distribution of particularly boron and titanium concentration. The difference in hardness of the microstructures is specifically attributed to the type of borides. The type, dimension, and the volume concentration changes of borides were correlated with the parameters as the concentration of additives and the dilution from the base material. The surfaces were subsequently characterized by scanning electron microscopy (SEM), the energy dispersive X-ray spectrometry (EDS), X-ray diffraction (XRD), and differential thermal analysis (DTA).

Introduction

Titanium diboride (TiB_2) is the most inert and hardest of all the borides [1]. TiB_2 is a hard material with a high resistance to wear and high tensile strength at high temperatures. The high density combined with the compressive strength and the high modulus of elasticity leads to its use in shielding elements. It resists against most reagents. It can be used to reinforce Fe-based composites by GTAW [2, 3]. Particle reinforced iron-based composites are produced mainly by powder metallurgy routes [4]. Fe-based metal matrix composites find extensive applications in tools, dies, and wear as well as high temperature oxidation-resistant components. Ceramic particulate-reinforced Fe-based composites are produced mainly by powder metallurgy routes involving the addition of ceramic powders to iron alloy powders [5–8]. Powder metallurgy has good surface quality and precision of products; on the other hand, the production of a surface having homogeneous mixing of ceramic particulates on a ferrous substrate is difficult by powder metallurgy process, and powder surfaces can easily be contaminated during mixing. Recently, in situ synthesis of TiB_2 particle-reinforced metal matrix composite-coated surfaces, which were produced by using GTAW, received much interest worldwide [3, 6]. These new techniques eliminate interfacial incompatibility of matrices with reinforcements based on their nucleation and growth from the parent phase. It is desirable that the surface layer of components is reinforced by TiB_2 particles to offer high wear resistance to them while they retain the high toughness and strength. GTAW has a potential to be used for surface modification [9]. There are many investigations on the surface coatings by laser or electron beam alloying and plasma alloying with powders having strong carbide- or boride-forming elements [10–14]. In this investigation, different from other studies, the reinforcement powders were synthesized as the initial powders consisting of B_2O_3 and Al, alloyed with FeTi, FeCr, and FeW. During synthesizing, Al reacts with B_2O_3 and then FeTi–FeW–FeCr ferroalloys react with B, thus promoting the formation of

S. O. Yilmaz (✉)
Faculty of Engineering, Department of Metallurgical and Materials Engineering, Fırat University, Elazığ, Turkey
e-mail: osyilmaz@firat.edu.tr

M. Ozenbas
Department of Metallurgical and Materials Engineering, Middle East Technical University, Ankara, Turkey

the desired transition metal borides. Boron and molten Al form above the eutectic temperature, this promotes liquid phase sintering. The reactions occur between 900 and 1100 °C [2]. It is aimed to obtain the phase transformations of the coated surfaces, which forms with boride reinforcing as evenly depositing alloy powders on an AISI 4340 steel substrate by means of GTAW process.

Materials and experimental procedures

A mixture of ferrotitanium, ferrotungsten, and ferrochromium ferroalloy powders were used with pure Al and boron oxide B_2O_3 powders. Rectangular plates of low carbon steel AISI 4340 (120 mm long, 50 mm wide and 10 mm thick) were used as substrates in a quenched and tempered condition. The surfaces of the samples were thoroughly cleaned, dried, and finally rinsed by acetone. The main chemical composition of FeTi, FeCr, FeW, B_2O_3, and Al powders are listed in Table 1, and the ratio of reinforcement particulates used for coating are listed in Table 2. The average size of the powders was in the range of 40–60 μm and appears to be in spherical shape. In order to obtain homogeneous mixing, the combined powders were attrition-milled for 1 h using agate ball mill with an agate container and the balls were operated at 300 rpm. The milled mixture with a thickness in the range of 0.5–2 mm was pre-coated on the surface of the substrate. Coating was conducted by using GTAW process, and a tungsten electrode of 2.4-mm diameter was used to produce a stable arc. The arc speed was applied as 25 mm/s. Pure argon was used as a shielding gas and the flow rate of argon was 8 L/min. The energy given to the surface was controlled as 5 J/cm^2 (Table 3).

Table 1 Chemical composition of reinforcements (wt%)

	W	Al	Ti	Si	%S	Fe	Cr	Mn	C	%P
FeTi		1.67	72	0.18	0.03	oth.				0.03
FeCr				1	0.04	oth.	70		0.1	0.04
FeW	77					oth.	0.5	0.16	0.07	0.04
B_2O_3	95% purity, other H_2O									
Al	99.9% purity									

Table 2 The ratio of reinforcement particulates used for coating (wt%)

Sample	FeTi	Al	B_2O_3	FeW	FeCrC
S1.1	80	10	10	–	–
S1.2	70	20	10	–	–
S1.3	70	10	20	–	–
S1.4	60	20	20	–	–
S2.1	80	5	5	10	–
S2.2	70	5	5	20	–
S3.3	60	10	10	20	–
S3.1	70	5	5	10	10
S3.2	60	5	5	20	10
S3.3	50	10	10	20	10

The samples were prepared for metallographic examination by grinding on SiC wheels followed by polishing and etched with nital (2% nitric acid). The observation and characterization of metallographic structure were performed using optical microscopy. The configuration of the borides was observed by CSM 950 scanning electron microscopy (SEM). Further phase characterization of the samples was undertaken by XRD in a MXP21VAHF diffractometer using cobalt Kα radiation. The thermodynamic of the borides were investigated by differential thermal analysis (DTA). Leica Q550 digital image analyzer with microprocessor was used to determine the borides volume fraction and particle size.

The abrasive wear tests were performed using a pin-on-disc type apparatus. Before the wear tests, each specimen was ground to grade 1200 abrasive paper. Abrasive wear tests were carried out under the load of 20, 40, 60, and 80 N on a grade 80 abrasive paper attached to the grinding disk, which rotated at 320 rev min^{-1}. A fixed track diameter of 160 mm was used in all the tests, and the duration of the abrasion test was 60 s. Each test was performed with a fresh abrasive paper, and, for each test condition, a minimum of three runs were performed. Wear loses were obtained by determining the masses of the samples before and after wear tests. The wear rates were calculated by converting the mass loss measurements (to the nearest 0.1 mg) to volume loss by using the respective densities:

$$W\left(\mathrm{mm^3\ m^{-1}}\right) = \frac{\text{mass loss (g)}/\text{density (g mm}^{-3})}{\pi \times 160 \times 10^{-3} \times 320(\mathrm{m})} \quad (1)$$

Results and discussion

Microstructure of coating

The exothermic dispersion process technology [15] was used with GTAW process to produce a new modified surface in the form of composites having TiB_2 reinforcement particulates. This process utilizes a mixture of powders of the ferroalloy powders components with a third metallic component. Heating of this mixture results in exothermal interaction between the components. Through these reactions, fine hardening particles can form in the solvent phase as 20-75 vol.%. In some studies [15–17], where Ti–B–Al is used, the particulates result in the formation of TiB_2 with a

Table 3 The effects of process parameters on the coating geometry

Process parameters				Coating size (μm)			
Electrode diameter (mm)	Process speed (mm/s)	Powder feeding (g/s)	Heat input (J/cm^2)	d_c	h_c	t_c	w_c
2.4	25	1.5	5	260	320	570	400

d_c = Maximum deepness (above the original substrate surface, h_c = max height above the original substrate surface, t_c = Maximum total coating thickness (=d_c + h_c), w_c = maximum width

size of 1–10 μm. For the FeTi–Al–B_2O_3 system, four reactions of reinforcements can form during the process:

$$Al_{(s)} = Al_{(l)} \quad (I)$$

$$FeTi_{(s)} + 3Al_{(l)} = Al_3Ti_{(s)} + Fe \quad (II)$$

$$FeTi + B_2O_3 + Al = TiB_2 + Al_2O_3 + Fe \quad (III)$$

$$B_2O_3 + Al + Fe = Fe_2B + Al_2O_3 \quad (IV)$$

The reaction III proceeds continuously during GTAW. The amount of B_2O_3 determines the concentration of TiB_2. During synthesis, Al consumes oxygen of B_2O_3 by reaction III and IV forming Al_2O_3 of slag [15]. Ti forms TiB_2 and the Ti left over in the structure may form TiB [15]. Figure 1 shows the representative microstructures of the surface coatings of sample $S_{1.1}$. The thickness of modified surface was seen as 1–3 mm Fig. 1a. Although, some areas show more Fe_2B particles as accumulated, the distribution of Fe_2B phase is, in general, uniform in the matrix of ferrite phase. In the surface of specimen S_{11}, uniform Fe_2B dispersions of 32 vol.% were achieved with particles size in the range of 3–5 μm (Fig. 1b). All of the Fe_2B phase is formed as intergranular form. This distribution of boride phase may be ascribed to the interaction between the particles and the advancing solid–liquid and liquid–liquid interface. The rapid movement of the solid/liquid interface limits in situ synthesis of Fe_2B particles, and brings about a uniform distribution. In addition, with an increase in the local interface solidification speed, some of Fe_2B particles are pushed and trapped by the solid–liquid interface.

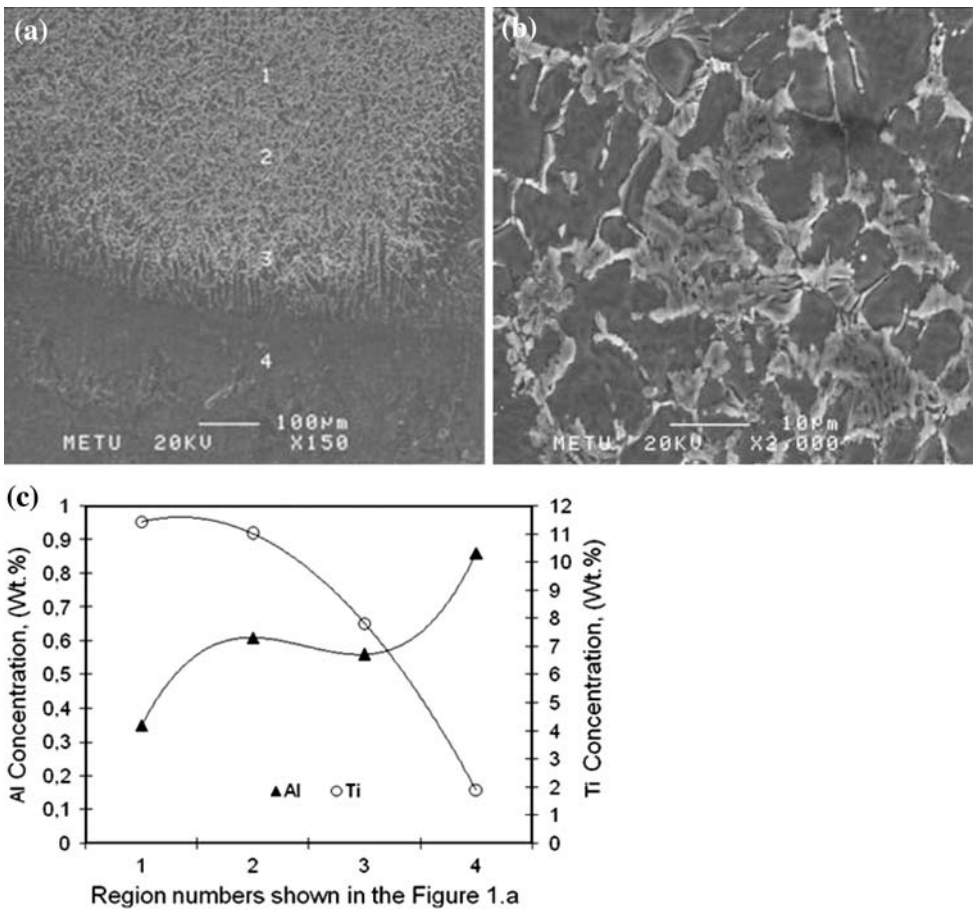

Fig. 1 SEM micrographs of S_{11}. group samples, **a** Cross-sectional micrograph showing coated surface and steel. **b** Coated surface, **c** Concentration change of Ti

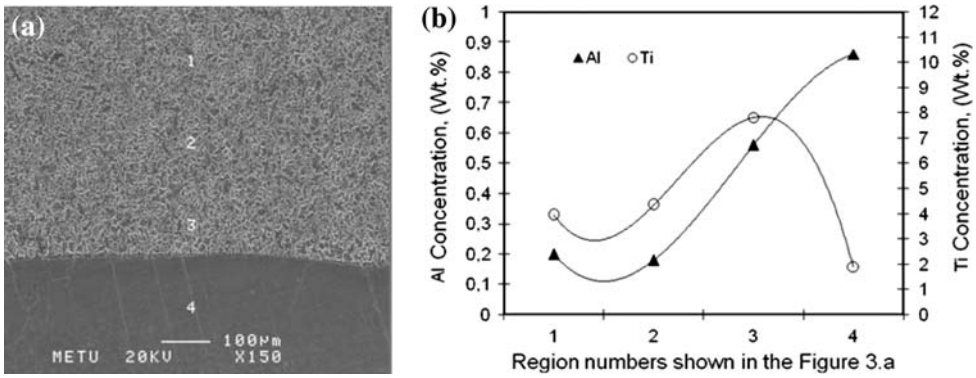

Fig. 2 **a** SEM micrographs of sample S_{12}, **b** Concentration change of Ti

Figure 2 shows the microstructures of the surface coatings of sample S_{12}. Depending on metallographic investigations, the matrix is ferrite (α-Fe) and the second phase is Fe_2B boride for the samples coated by the cladding material (FeTi + Al + B_2O_3). It is seen from elemental distribution that Ti concentration decreased coming closer from coated surface to the steel side, and TiB_2 borides could not be observed in the microstructure of sample $S_{1.2}$ (Fig. 2b). We have changed the concentration of coated powder material for sample $S_{1.3}$. Al ratio decreased from 20 to 10 wt%, and the B_2O_3 ratio increased from 10 to 20 wt% (Table 2). The micrographs of the sample $S_{1.3}$ was given in Fig. 3a. EDS analysis shows that the concentration change of cladding powder material decreased the concentration of Ti in coating surface, but TiB_2 phase could not be observed in the microstructure of sample $S_{1.3}$ (Fig. 3b).

In some studies, (Ti, Al)B_2 or AlB_2 and TiB_2 phases can form during Fe–Al–Ti–B systems; on the other hand, Fe_2B phase was observed at TiB_2–Fe systems [15–18]. The fracture toughness of Fe_2B and AlB_2 borides is not sufficient for wear applications. For this reason, the chemical composition of coating material must be adjusted appropriately to obtain also TiB_2 phase. Tungsten was added to the cladding material as ferrovolfram (FeW) to help the formation of TiB_2 phase [19], and the coated samples having W were called as S_2 group (Table 2). The micrographs of the coated surfaces of group S_2 samples were given in Figs. 4 and 5. XRD pattern of the surface composite coatings is shown in Fig. 4c, which indicates that the phases present in the coating are mainly spherical TiB_2, α-Fe, and Fe_2B intermetallic compounds. The intermetallic compounds forming interdendritically during the late stages of solidification. It clearly confirms that TiB_2 particulates can be synthesized by direct reaction between FeTi, Al, and B_2O_3 at presence of 10 wt% FeW. Depending on the EDS analysis, it was seen that W matrix was seen as 0.2 wt% and, rather it is found as dissolved in hard boride particulates as 0.6–0.7 wt% (Tables 4, 5). A small change of Ti ratio changes the chemical composition of liquid solution causing a shift in the structure from TiB_2–Fe binary phase equilibrium to TiB_2–Fe–Fe_2B. It is seen from the Tables 4, 5 that the chemical composition of Ti in TiB_2 phase decreased from 78 wt% to 40 wt% by decreasing the ratio of FeTi powders from 80 wt% to 70 wt% (Table 2).

Chromium was added to cladding complex material as ferrochromium (FeCr) to increase the ratio of TiB_2 phase [19]. FeCr was chosen instead of pure Cr because its melting temperature is low (1600 °C). The samples coated with cladding material containing FeCr was called as S_3 group. The SEM micrographs of the coated surface of group S_3 samples that were coated with cladding powders

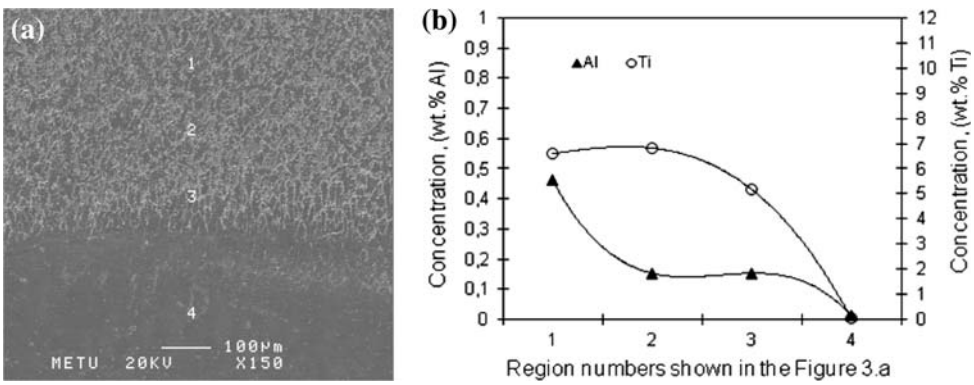

Fig. 3 **a** SEM micrographs of sample S_{13}, **b** Concentration change of Ti and Al

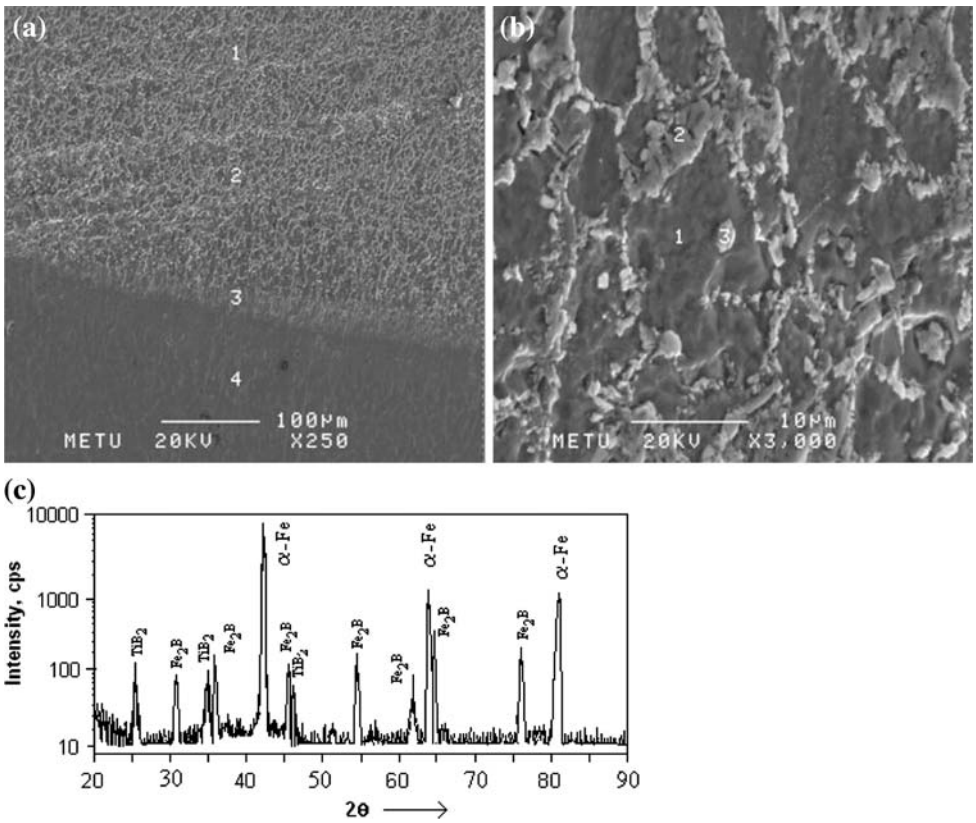

Fig. 4 SEM micrographs of sample $S_{2.1,}$ **a** Cross-sectional micrograph showing coated surface and steel together, **b** Coated surface, **c** X-ray diffraction pattern of coated surface

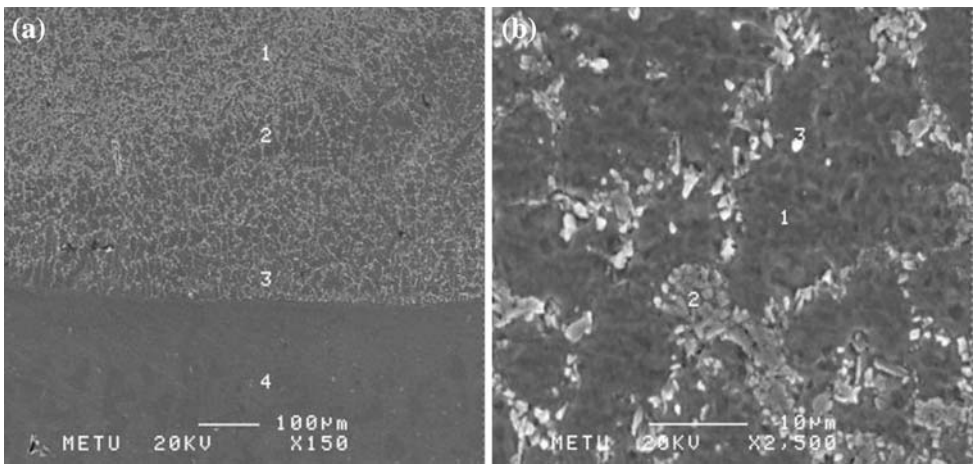

Fig. 5 SEM micrographs of sample $S_{2.2}$, **a** Cross-sectional micrograph showing coated surface and steel together, **b** Coated surface

Table 4 EDS analysis of sample $S_{2.1}$taken from the SEM micrographs given in Fig. 4

		Al	Ti	Si	Cr	W	Mn	Fe
Micrograph 4.a	1. Region	0.77	3.85		0.61	0.43		94.33
	2. Region	0.40	18.42		0.64			80.54
	3. Region	0.50	6.67		0.3	0.13		92.40
	4. Region			0.48			1.30	98.22
Micrograph 4.b	1. Region	0.82	15.99		0.58	0.20		82.40
	2. Region	0.35	12.23		0.44	0.69		86.29
	3. Region		78.02			0.64		21.34

Table 5 EDS analysis of sample $S_{2.2}$ taken from the SEM micrographs given in Fig. 5

		Al	Ti	Si	W	Mn	Fe
Micrograph 5.a	1. Region	0.48	9.10			1.59	88.83
	2. Region	0.24	6.18		0.12	1.76	91.70
	3. Region	1.97			0.49	1.86	95.68
	4. Region			1.11		1.66	97.23
Micrograph 5.b	1. Region	0.35	2.83		0.35	1.59	94.88
	2. Region	0.19	12.60		0.72	1.63	84.85
	3. Region	0.34	40.16		58.83		59.50

mixture of (FeW–FeCr–B_2O_3–Al–FeTi) are given in Figs. 6, 7, 8. As seen from the microstructure and EDS analysis (Table 6) that Cr and W elements were dissolved in the matrix. XRD pattern of the surface composite coatings is shown in Fig. 6c. It indicates that the existing phase of coated surface is mainly TiB_2 and α-Fe. The intermetallic compound Fe_2B was not observed for the samples coated by (FeW–FeCr–B_2O_3–Al–FeTi) powders mixture. The TiB_2 phase was formed homogenously and in spherical form. The borides having (900–1100 °C) melting temperature and appropriate wetting character were not formed. The diborides of IV–VI group metals dissolve at temperatures 2000–3000 °C, and the atomic size difference between the elements decreases the dissolution temperatures [20, 21]. For this reason, it is thought that W and Cr activated the formation of (Ti, Cr)B_2 at 2000 °C. The EDS analysis (Tables 6, 7, 8) showed that the hard particulates are (Ti, Fe)B_2 when the concentration of cladding powders have about 70 wt% FeTi. However, the decrease of FeTi powder concentration at cladding powders from 70 wt% to 60 wt% changed the type of the boride from (Ti, Fe)B_2 to (Fe, Ti)B_2 (Tables 6, 7, 8). The chemical analysis taken from the borides show that Ti concentration at hard particulates is 65 wt% for sample $S_{3.1,}$ 19.23 wt% for sample $S_{3.2}$, and 3.61 wt% for sample $S_{3.3}$. TiB_2 phase can be present with FeB, Fe_2B, α or γ-Fe, $FeTi_2$, and FeTi phases [21]. The presence of Cr in coated surface increases the nucleation rate of TiB_2 phase, and in this investigation, we have not seen Cr in hard boride phases (Tables 6, 7, 8). The borides which were formed by transition metals have lower melting temperature [21]. The samples having W have shown that W decreased the hard phase ratio; on the other hand TiB_2 hard phases were seen in these samples. Three types of borides, (Ti, W)B_2, (Ti, Cr, W)B_2, and (W, Ti)$_2B_5$, can form at Cr–Ti–W–B system [18]. However, (Ti, Cr, W)B_2 phases could not be observed for samples $S_{3.1}$–$S_{3.2}$–$S_{3.3}$ in this study. The best material balance for maximum TiB_2 and minimum FeB_2 phases was seen as the composition of $S_{3.2}$.

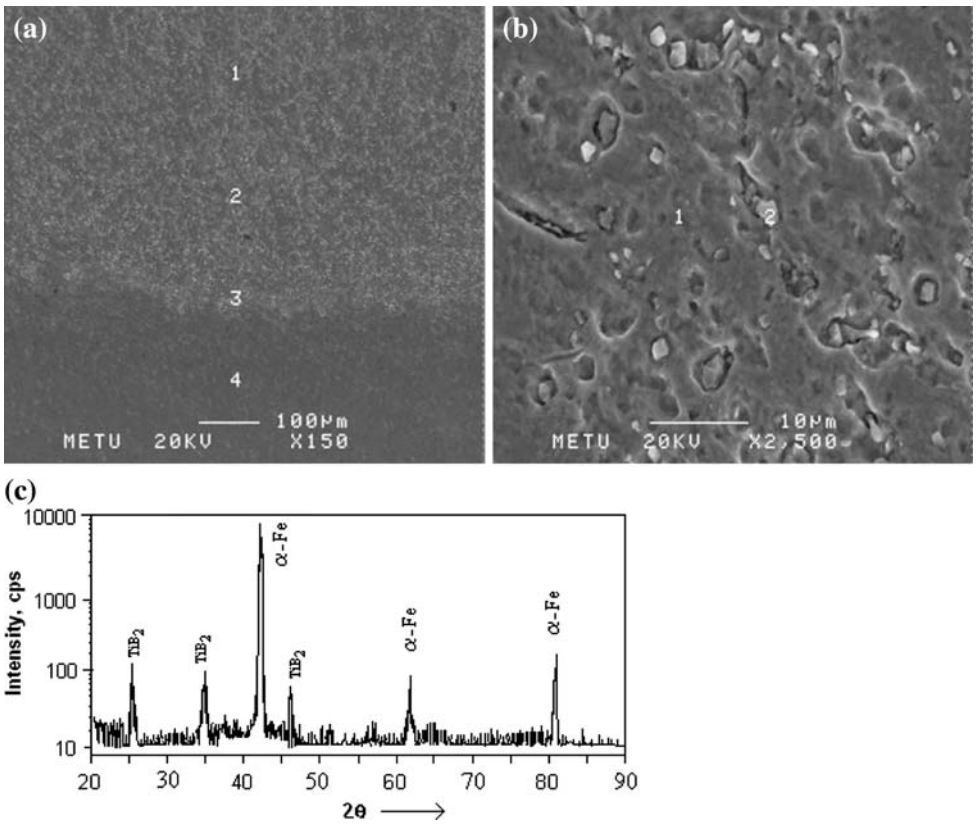

Fig. 6 SEM micrographs of sample $S_{3.1}$, **a** Cross-sectional micrograph showing coated surface and steel together, **b** Coated surface, **c** X-ray diffraction pattern of coated surface

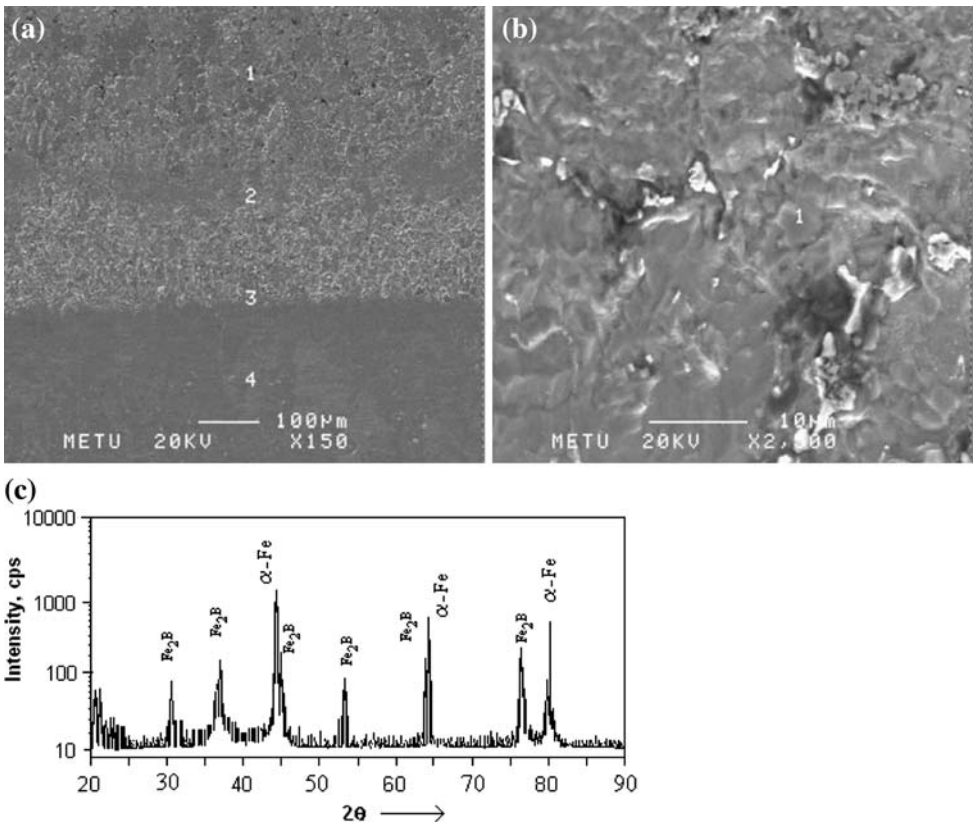

Fig. 7 SEM micrographs of sample $S_{3.2}$, **a** Cross-sectional micrograph showing coated surface and steel together, **b** Coated surface, **c** X-ray diffraction pattern of coated surface

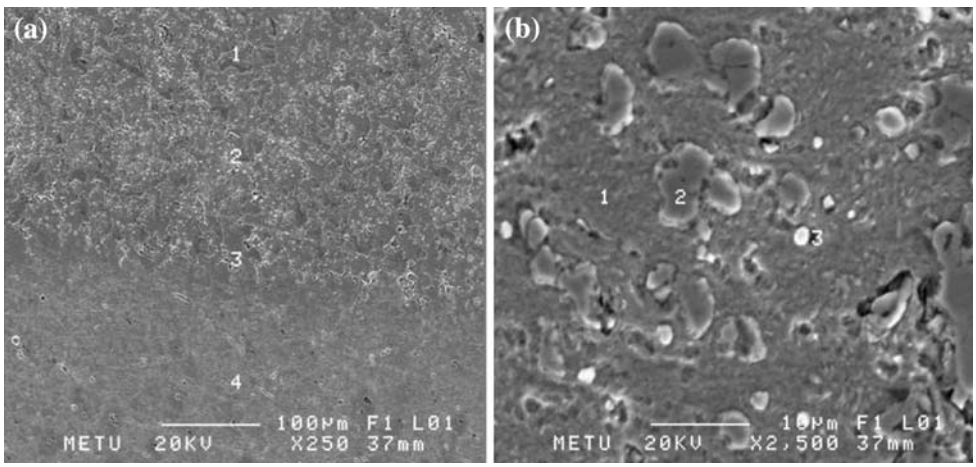

Fig. 8 SEM micrographs of sample $S_{3.3}$, **a** Cross-sectional micrograph showing coated surface and steel together, **b** Coated surface

Table 6 EDS analysis of sample $S_{3.1}$ taken from the SEM micrographs given in Fig. 6

		Al	Ti	Si	Cr	W	Mn	Fe
Micrograph 6.a	1. Region	0.39	4.76				1.22	93.63
	2. Region	0.47	5.88		0.05		1.01	92.58
	3. Region	0.17	4.93			0.77	1.07	93.06
	4. Region			0.39			1.07	98.54
Micrograph 6.b	1. Region	0.37	0.90		0.02	2.09	0.93	95.74
	2. Region		65.59					34.41

Table 7 EDS analysis of sample $S_{3.2}$ taken from the SEM micrographs given in Fig. 7

		Al	Ti	Si	Cr	W	Mn	Fe
Micrograph 7.a	1. Region	0.11	2.12		0.12	0.23	1.77	95.64
	2. Region	0.24	1.85		0.04		1.55	96.31
	3. Region		1.02				1.55	97.43
	4. Region			1.15			1.88	96.96
Micrograph 7.b	1. Region	0.03			0.06		1.88	98.03
	2. Region		19.23			0.20	1.32	79.25

Table 8 EDS analysis of sample $S_{3.3}$ taken from the SEM micrographs given in Fig. 8

		Al	Ti	Si	Cr	W	Mn	Fe
Micrograph 8.a	1. Region	0.15	2.26		0.15	0.48		96.96
	2. Region		2.49		0.25			97.26
	3. Region		1.45		0.27			98.27
	4. Region			0.37			1.44	98.19
Micrograph 8.b	1. Region	0.18	1.03					98.79
	2. Region	0.11	1.71		0.11			98.07
	3. Region	0.25	3.61		0.13			96.01

DTA of the coating

The enthalpy changes and dissolution temperatures of the samples were shown in Table 9. DTA of group S_1 samples shows that γ-Fe phase transforms to α-Fe phase during 759–1050 °C temperatures. The dissolution temperature of F_2B phase was found as 1120–1270 °C. The decrease of B_2O_3 rate of coating powders to 5 wt% and addition of FeW as 10 wt% to coating powders increased the transformation temperature of γ-Fe to 1128 °C (Sample $S_{2.1}$).The decrease of FeTi concentration in coating powders from 80 to 70 wt% decreased the transformation temperature of γ-Fe from 1128 °C to 914 °C ($S_{2.1}$–$S_{2.2}$). On the other hand, FeW powders addition to cladding material did not affect the dissolution temperatures of Fe_2B phase. The addition of FeCr powders with FeW powders to cladding material decreased the transformation temperatures of γ-Fe to α-Fe slightly ($S_{3.1}$–$S_{3.2}$). Furthermore, the enthalpy change of this transformation reaction increased from −2430/4000 to −7200/13390 J/g mol. (Table 9). The DTA and XRD results of this study are in good agreement with some researches [21–23]. The transformation temperatures of γ-Fe to α-Fe for S_3 group was similar to S_2 group. However, we have not detected the Fe_2B dissolution for sample $S_{3.1}$. DTA results show that there is no change in microstructure due to dissolution of Fe_2B and TiB_2 particles of the coated surfaces. Therefore, these coated surfaces can be expected to be stable at high temperatures. Finally, TiB_2 phase is at equilibrium with FeB_2, and α-Ti below 1100 °C. Over 1340 °C, TiB_2 phase is stable with γ-Fe, and liquid Fe phase. Between 1100 and 1300 °C temperatures, Fe_2B phase is stable.

Table 9 DTA analysis of samples giving dissolution temperatures and enthalpy changes

Sample	γFe → αFe		Fe_2B → Liquid	
	T °C	ΔH J/g mol	T °C	ΔH J/g mol
$S_{1.1}$	840	−3360	1240	−23
$S_{1.2}$	759	−4650	1120	−2.4
$S_{1.3}$	1058	−779	1272	−5.9
$S_{2.1}$	1128	−4000	1230	−5.9
$S_{2.2}$	914	−2430	1289	−37.8
$S_{3.1}$	1036	−7200		
$S_{3.2}$	1123	−13390	1292	−1.82

Hardness of the coating

The microhardness of the coated surface reinforced by TiB_2 and Fe_2B particles was determined along the depth from the irradiated surface; all the data were an average of three measurements. The variation of the microhardness across the transverse cross section of the coating are presented in Fig. 9 demonstrating that the presence of FeW and FeCr in the cladding material produce an increase in microhardness due to solid solution strengthening, and an increase of TiB_2 with Fe_2B hard phase ratio. The microhardnesses of the hard particulates and matrix were shown in Table 10. The microhardness of the coating progressively decreased from the surface to the substrate. It is noted that there is no sudden transition from the coating to the substrate in the

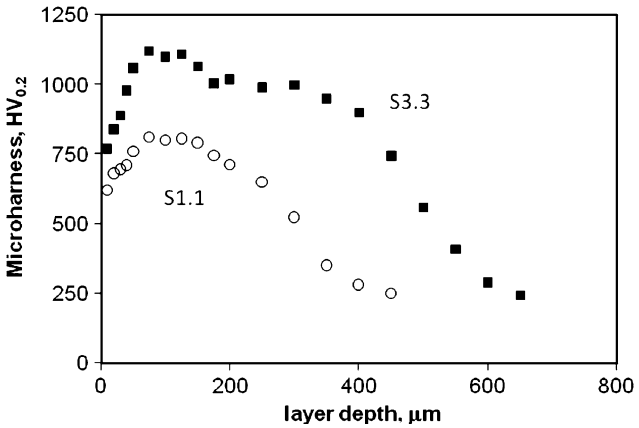

Fig. 9 Microhardness via layer depth of the GTA processed coating of S_{11} and S_{23}

hardness, which indicates an absence of a sharp demarcation in materials properties across the interface. Furthermore, average microhardness of coating gradually increased with the increase in content of TiB_2 and Fe_2B, which was due in part to the formation of more particles during GTAW processing. The highest hardness value was obtained from the coated sample having a 39 vol.% hard phase ratio. The matrix hardness also changed depending on the chemical concentration. The reported hardness value of TiB_2 vary from 2900 HV [22] to 3400 HV [23]. The measured hardness value of TiB_2 falls within the reported range. The measured hardness of Fe_2B matches with the literature value [24, 25].

Wear characterization of the coatings

The abrasive wear results for the coatings are given in Fig. 10. The figure emphasizes the role of applied load between wear rate and loading in a linear function. A material's wear-resistance property is not identified by hardness alone. It also depends on microstructural parameters like volume fraction, size, shape, and distribution of embedded particles, properties of matrix, and the interfacial bonding between the two phases [25]. The overall depth of the plastic deformation related linearly to the applied load and the grit dimensions. The tribological behaviors depend on the microstructural properties of the material and type of loading-contact situation [5]. Considering Fig. 10, the sample $S_{1.3}$ having the highest B and Al demonstrates a lower wear rate than other samples of S_{11} and S_{12}. This wear rate difference for the samples S_1 group is attributed to the content of boride volume fractions and boride sizes in the matrix of the surfaces. The sample S_{23} show the lowest wear rate for sample group of S_2 (Fig. 10b) and the sample $S_{1.3}$ show the lowest wear rate of the sample group of the S_3 (Fig. 10c). The lowest wear rate was seen from the sample $S_{1.3}$ among all of the samples.

The hardness of TiB_2 particles in the surface is higher than 3000 HV. Khrushov et al. [26] suggest that higher the hardness of the reinforcing particle, better the wear resistance. Both TiB_2 and Fe_2B phases present in the coated surface may act as reinforcements in the composite. The mechanical and tribological properties of the coatings having composite structure depend strongly on the type of matrix phases, grain size, distribution of hard phases, and chemical concentration. A close relation between wear rate and particulate size was detected (Fig. 11a). The wear behavior operates differently depending on the orientation of the borides with respect to the wear surface of coating. In the specimens with the borides oriented transverse to the abrasion direction, and with the long axis of the borides perpendicular to the wear surface the borides bend and fracture very near the surface. In this case, it was considered that the tangential forces applied by the moving abrasive particles caused bending. During bending, tensile stress develops on the backside of boride, leading to fracture. However, as the boride size decreases, bending and fracture become more difficult under the same applied tangential force. The wear rate decreases with a decrease of Ti level in hard phases, and this means that the wear rate decreases with boride volume fraction, and with boride size at the same boride volume fraction. The relationship between wear rate and the boride volume fraction for each sample is illustrated in Fig. 11b. Consequently, it can be said that harder borides (TiB_2) in structures appear more resistant to deformation and fracture. The concentration of

Table 10 The hard phase ratio, surface hardness, and microhardness of hard phases and matrix of coated surfaces

Sample	TiB_2 HV	Fe_2B HV	Hard phase ratio vol.%	Matrix HV	Surface hardness HRC
$S_{1.1}$		1550–1700	31.0	670–700	44.27
$S_{1.2}$		1600–1700	32.7	800–900	47.8
$S_{2.1}$	2700–3000	1500–1700	30.2	800–1000	44.1
$S_{2.2}$	2300–2400	1300–1450	30.6	800–1000	45.9
$S_{3.1}$	2700–3300		33.2	800–1000	49.9
$S_{3.2}$		1100	39.4	900–1100	53.7

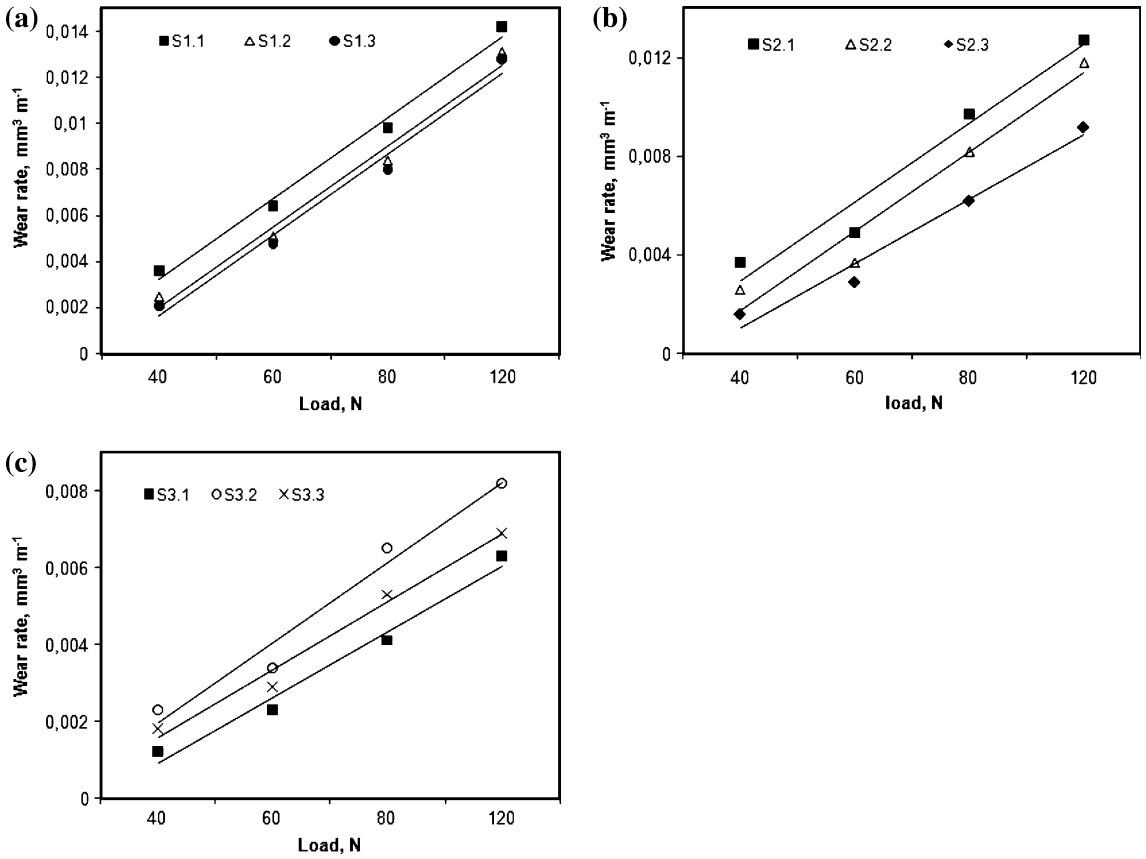

Fig. 10 The wear rate vs. load for a sliding distance of 800 m and a sliding speed of 0.84 m s^{-1} **a** S_1 group, **b** S_2 group, **c** S_3 group

borides changed at matrix of the samples, and the difference of the concentration has brought a difference in wear behavior, has changed from matrix to the borides. It is considered that the abrasive wear results can form an opinion about the effect of the boride volume fraction on wear behavior and wear resistance of the coated surfaces [19]. The decrease of the wear rate with increasing hard phase volume fraction could be obtained [6].The relationship between hardness and wear rates is given in Fig. 11c. As seen from the figure, a close relationship was seen between hardness and wear rate. Comparison between the change of Ti in the matrix of the samples shows that, for a significant increase in the Ti concentration promotes the formation of thicker and harder coatings and melted regions below the original surface with negligibly small thickness. Therefore, the surfaces having high TiB_2 and low Fe_2B are expected to be more resistant to abrasion. It can be concluded that, the boride structure in these coated surface is un-influential on abrasive tribo-environment. In addition, the nature of the matrix surrounding the boride has also a profound effect on the performance of borides. The results of this study clearly demonstrate that while the orientation of borides in the wear of samples having Fe_2B microstructure influences the wear rate significantly.

The relationship between dissolution temperature of matrix and wear rate, and enthalpy change versus wear rate of samples are shown in Fig. 11d, e, respectively. A progressive relationship is present between wear rate and matrix dissolution temperature-phase transformation enthalpies. As the dissolution, temperature and enthalpies increases wear rate decreases. During wear process, a large energy releases and the temperature of the surface increases. Hence, a material having high wear resistance must have a high dissolution temperature with dissolution enthalpy, showing the stability of the matrix. It is known that TiB_2, having very high specific modulus, supports the load bearing capacity.

Conclusions

1. A new in-situ method has been developed to produce TiB_2 and Fe_2B particles reinforced Fe-based alloy surface coating.
2. TiB_2 phase could not be observed in the microstructure of the sample group S_1. Fe_2B phase is formed at 3–5 μm size, ≈32 vol.% and as intergranular form in the microstructure.

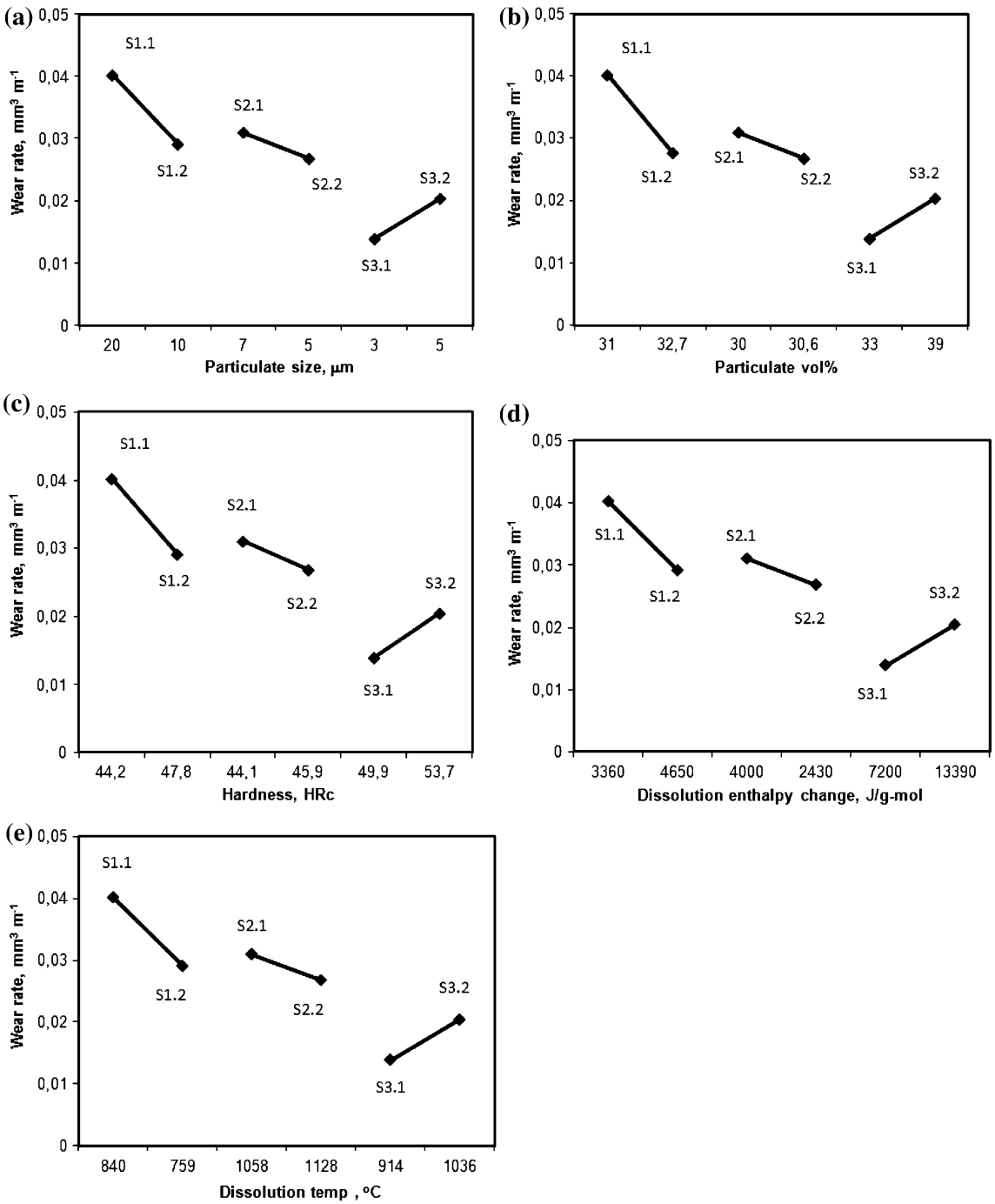

Fig. 11 Relationship between **a** wear rate and particulate size, **b** wear rate and particulate vol.%, **c** wear rate and hardness, **d** abrasion resisitance and dissolution temperature, **e** abrasion resisitance and enthalpy change of γ–α phase transformation of sample groups. (Normal load 140 N, sliding distance of 800 m and a sliding speed of 0.84 m s^{-1})

3. The intermetallic compounds are mainly spherical TiB_2 and interdendritical Fe_2B for the sample group S_2 having Ti with W as boride forming elements. X-ray diffraction patterns of the surface composite coatings of group S_2 samples showed that the existing phases in the coating were mainly $\approx$30 vol.% TiB_2, and Fe_2B intermetallic compounds.

4. Both Cr and W elements were dissolved in the matrix of sample S_3. The presence of W and Cr increased the transformation temperature and transformation enthalpy of γ-Fe to α-Fe phase. TiB_2 and Fe_2B phases enhanced the hardness of the composite coatings. The highest TiB_2 concentration was seen for the sample S_{31} having the phases mainly $\approx$35 vol.% TiB_2 and 65vol.%

α-Fe. The intermetallic compound Fe_2B was not seen for this sample coated by FeW–FeCr–B_2O_3–Al–FeTi cladding powders mixture. The samples S_{31} show the highest hardness and the lowest wear rate.

Acknowledgements The authors gratefully acknowledge the assistance the committee of scientific research/TÜBİTAK for its support of this research (grant No.105m355/2007). The authors would like also to gratefully acknowledge the use of laboratory facilities at METU and Firat University, Türkiye.

References

1. Laird G, Gundlach R, Rohrig K (2000) Abrasion-resistant cast iron handbook. American Foundry Society, Illinois, p 72
2. Lörcher R, Telle R, Petzow G (1988) Mater Sci Eng 105–1061:117
3. Wang XH, Song SL, Qu SY, Zou ZD (2007) Surf Coat Tech 201(12):5899
4. Cheol Kim H, Oh D-Y, Guojian J, Shon I-J (2004) Mater Sci Eng A 368(1–2):10
5. Tjong SC, Lau KC (2000) Mater Sci Eng A 282(1–2):183
6. Wang XH, Zhang M, Zou ZD, Song SL, Han F, Qu SY (2006) Surf Coat Tech 200(20–21):6117
7. Rai VK, Srivastava R, Nath SK, Ray S (1999) Wear 231(2):265
8. Raghunath C, Bhat MS, Rohatgi PK (1995) Scr Metall Mater 32(4):577
9. Yılmaz SO (2005) Surf Coat Tech 194:175
10. Pons M, Gharnit H, Galerie A, Caillet M (1988) Surf Coat Tech 35(3–4):263
11. Yi Z, Shao G, Duan X, Sun P, Shi X, Xiong Z, Guo J (2005) China Particuol 3(5):286
12. Shafirstien G, Bamberger M, Langohr M, Maisenhalder F (1991) Surf Coat Tech 45(1–3):417
13. Tayal M, Mukherjee K (1994) Mater Sci Eng A 174(2):231
14. Agarwal A, Narendra B (2000) Wear 240(1–2):144
15. Goldfarb I, Bamberge M (1996) Scr Mater 34(7):1051
16. Zeng Z, Zhang J (2008) Surf Coat Tech 202(12):2725
17. Satyaprasad K, Mahajan YR, Bhanuprasad VV (1992) Scr Metall Mater 26(5):711
18. Petzow G, Telle R, Danzer R (1991) Mater Charact 26(4):289
19. Yılmaz SO (2007) Tribol Int 42:6769
20. Nıshıyama K, Umakawa S (1990) In: Kobayashi A (ed) Achievements in composites in Japan and the United States. Proceedings of the 5th Japan-US Conference on Composite Materials, Tokyo, pp 371–378
21. Jüngling TJ, Sigl LS, Oberacker R, Thümmler F, Schwetz KA (1993–1994) Int J Refract Met Hard Mater 12(2):71
22. Hilz G, Holleck H (1991) Mater Sci Eng A 139:268
23. Terry BS, Chinyamakobvu AS (1992) Mater Sci Technol 8:491
24. Degnan CC, Shipway PH (2002) Metal Mater Trans A 33:2973–2983
25. Pagounis E, Talvitie M, Lindroos VK (1997) Powder Met 40:55
26. Khruschov MM (1974) Wear 69:69